INTERNATIONAL JOURNAL OF CLIMATOLOGY
Int. J. Climatol. **38**: 1692–1705 (2018)
Published online 15 September 2017 in Wiley Online Library
(wileyonlinelibrary.com) DOI: 10.1002/joc.5289

Year-to-year variability of surface air temperature over China in winter

Dong Xiao,[a] Zhiyan Zuo,[a,b]* Renhe Zhang,[c] Xingyu Zhang[d] and Qiong He[e]

[a] *State Key Laboratory of Severe Weather, Chinese Academy of Meteorological Sciences, Beijing, China*
[b] *Collaborative Innovation Center on Forecast and Evaluation of Meteorological Disasters, Nanjing University of Information Science & Technology, China*
[c] *Institute of Atmospheric Sciences, Fudan University, Shanghai, China*
[d] *School of Mathematical Sciences, University of Science and Technology of China, Hefei, China*
[e] *Earth System Modeling Center and Climate Dynamics Research Center, Nanjing University of Information Science & Technology, China*

ABSTRACT: In this study, the year-to-year variability of surface air temperature (SAT) over China in winter was investigated during 1961–2014. The results indicate that the year-to-year SAT variability can explain more than 30% of the SAT variance over most parts of China, with up to 60% variance over southern China, northeastern China and northwestern China. The leading pattern of year-to-year SAT exhibits homogeneous variability over most parts of China, except in small areas over the Tibetan Plateau and southwestern China. The circulation over the northern Pacific is a key factor of this homogeneous variability pattern. An anomalous anticyclonic circulation and weakening midlatitude westerly jet in the middle and high troposphere over the northern Pacific are associated with the homogeneous warmth over China. The second pattern shows a south–north dipole, with variability in northeastern China opposite to that south of 25°N in China and over the Tibetan Plateau. The south–north dipole pattern is part of a global year-to-year SAT anomaly pattern because it exhibits a significant relationship with the year-to-year SAT over large parts north of 50°N over the Eurasian landmass. The north-cold/south-warm pattern is accompanied by a significant weakening of the Arctic Oscillation. In comparison, the atmospheric circulation anomalies associated with the homogeneous variability pattern are much weaker than those with the south–north dipole pattern. The anomalous Indian Ocean dipole in the previous autumn and the snow cover around China in November are the two key causes of the homogeneous variability pattern. Many factors, such as the tropical central Pacific sea surface temperature (SST), stratospheric quasi-biennial oscillation (QBO), Okhotsk sea ice and western Siberia snow cover, can significantly influence the south–north dipole pattern. Compared to the tropical Pacific SST, the impact of the Indian Ocean SST on the winter SAT over China is much more important.

KEY WORDS year-to-year variability; surface air temperature; China; winter

Received 24 April 2017; Revised 26 July 2017; Accepted 17 August 2017

1. Introduction

In the recent decades, research on global surface air temperature (SAT) has become a focal point because of global warming. Over China, previous studies have paid great attention to warming trends and variation in decadal-to-interdecadal time scales (Xiao *et al.,* 2012; Zhao *et al.,* 2014). However, the SAT variation at shorter than decadal time scales, such as interannual variability, is very intensive and more important for weather forecasting and seasonal climate predictions. The prediction of winter SAT over China is one of several important tasks of the Chinese Meteorological Administration. Previous studies have demonstrated the interannual variability of SAT over China. For example, Kang *et al.* (2009) documented that the leading pattern of SAT over China exhibits homogeneous variation, while the second pattern shows a south–north dipole feature on interannual time scales. A strong (weak) East Asian winter monsoon (EAWM) generally corresponds to a cold (warm) land surface over China in the winter (Yang *et al.*, 2002; Zhu, 2008; Wang and Fan, 2013). As China is part of the EAWM domain, research on SAT over China is generally not limited to China but covers the whole EAWM domain. Wang *et al.* (2010a) reported that there are two major modes of SAT over the southern EAWM domain (0°–30°N, 100°–140°E) and the northern EAWM domain (30°–60°N, 100°–140°E), respectively. Sun *et al.* (2016) considered the EAWM domain as a whole and indicated major intensive interannual variability of SAT in the first mode over the northern part of the EAWM domain and a second mode over the southern part of the EAWM domain. On a continental scale, the interannual variation of springtime Eurasian SAT exhibits a north–south seesaw spatial pattern (Shen and Kimoto, 2007). Therefore, the variability of SAT over China may not only be related to the SAT over EAWM domain but also to the SAT over other regions beyond the EAWM domain.

* Correspondence to: Z. Zuo, State Key Laboratory of Severe Weather, Chinese Academy of Meteorological Sciences, No. 46 Zhongguancun South Street, Beijing 10081, China. E-mail: zuozy@cma.gov.cn

That is, the leading patterns of SAT over China may be part of SAT variations at a continental or global scale.

Li and Long (1992) suggested that there is a quasi-biennial oscillation (QBO) in the temperatures over East China that exhibits a significant relationship with the stratospheric QBO. Chang and Li (2000) reported the existence of tropospheric biennial oscillation in the Asian climate. Chen and Li (2007) showed that significant warming occurs in northeastern Asia in the QBO easterly phase. Li *et al.* (2011) reported that there is a type of 2-year cycle in EAWM via the summer monsoon. The 2-year cycle variability is apparently an important feature in the variations of SAT over China. Furthermore, Fan (2009) described the approach using the year-to-year increment of a variable that had good prediction capability in seasonal climate forecasting, which includes the winter SAT over northeastern China. Wang *et al.* (2010b) further discussed the year-to-year increment approach with physical–mathematical considerations and validated the approach based on a climate model prediction experiment. A detailed analysis on the year-to-year variability of SAT over China may be beneficial for the improvement of predictive approaches to winter SAT over China. The question is what about the relation of 2-year cycle variability to the year-to-year variability over China?

Kang *et al.* (2009) reported that the first mode of interannual SAT variability over China is significantly related to the East Asian trough at 500 hPa and the north–south movement of the 200 hPa East Asian jet stream, whereas the second mode is related to the Arctic Oscillation (AO). They suggested that there is a significant impact of sea surface temperature (SST) over the tropical Pacific and northern Pacific on the two modes, which is consistent with previous studies (Zhang *et al.,* 1996). In addition to SST, other factors, such as the North Atlantic Oscillation (NAO), the AO and Tibetan Plateau snow cover, which were also illustrated, exhibit significant influence on the SAT variability over East Asia (Wadlland and Simmonds, 1997; Watanabe and Nitta, 1999; Gao and Yang, 2009; Gong *et al.,* 2001; Wu *et al.,* 2011; He *et al.,* 2017). Seager *et al.* (2010) reported that negative NAO and El Niño events are responsible for the Northern Hemispheric snow anomalies that occurred in the winter of 2009/2010. Zuo *et al.* (2015) documented that the AO exhibited a significant relationship with the SAT in southern China in the winter via the Middle East jet stream. He and Wang (2013) reported that the AO in November or December was significantly associated with the SAT anomalies over East Asian in January via Rossby wave activity. In recent decades, the impact of Eurasian snow cover and Arctic Sea ice on widespread winter cooling over midlatitudes has generated much research interest because of the rapid warming in the Arctic and its direct effect on Eurasian snow cover in the past decades (Budikova, 2009; Francis and Vavrus, 2012; Liu *et al.*, 2012; Li and Wang, 2013; Gao *et al.,* 2015). Huang and Gao (2012) illustrated the dominant pattern of the East Asian SAT and their significant relationship with sea ice. Barnes (2013) and Sceen *et al.* (2013) found a relationship of Arctic sea ice losses with the SAT over the Eurasian landmass. Sun *et al.* (2016) demonstrated a significant relationship between sea ice over the Arctic and the SAT over East Asia in the winter at interannual time scales. Focusing on the winter SAT over China at interannual time scales, what about the detailed contribution of the aforementioned factors on the dominant patterns of SAT variability over China? To address this question, we may shed light on the operational seasonal climate prediction of the winter SAT.

The purpose of this study was to investigate the interannual variability of winter (December–January–February) SAT over China in detail, with a focus on 2-year cycle variability, as this seems to be very important to interannual variability. What about the contribution of the 2-year cycle variability to interannual variability or to the total variations? Are the principal modes of winter SAT over China part of the SAT variability at a continental scale or not? What about the associated atmospheric circulation under these principal modes? Furthermore, what are the origins of these principal modes? We try to address these questions in this study. The data sets and methods are described in Section 2. In Section 3, we analysed the contribution of the 2-year cycle variability to the total variability, thereby evaluating the principle modes of 2-year cycle variability over China and their relationship to the SAT over other regions. The atmospheric circulation associated with these principal modes is depicted in Section 4, and the plausible causes of these principal modes are discussed in Section 5. A summary of the results is presented in Section 6.

2. Data and methods

The present analysis is based on observational monthly mean SAT data recorded at 386 meteorological stations in China from 1961 to 2014 that were provided by the Chinese Meteorological Administration. The atmospheric data derived from the National Centers for Environmental Prediction-National Center for Atmospheric Research (NCEP-NCAR) reanalysis are also used (Kalnay *et al.,* 1996). Furthermore, the improved extended reconstructed SST version 4 (Smith and Reynolds, 2004), the Hadley Center sea ice concentration data set (Rayner *et al.,* 2003), the satellite-based snow cover fraction data set provided by the Rutgers Global Snow Lab for 1966–2009 (Robinson *et al.,* 1993; Ramsay, 1998), the East Asian summer monsoon index (Li and Zeng, 2002, 2003, 2005; http://ljp.gcess.cn/dct/page/65577) and the QBO index (http://www.esrl.noaa.gov/psd/data/correlation/qbo.data) are used to investigate the plausible impacts on interannual SAT variability over China. The study period is 1961–2014, unless special denotation is provided. In this study, the year-to-year SAT is described by the difference of the SAT value in the following year from that in the present year (Wang *et al.,* 2010b).

The ensemble empirical mode decomposition (EEMD) method is used to extract the signals of SAT variations at various time scales for this study (Wu *et al.,* 2011). The

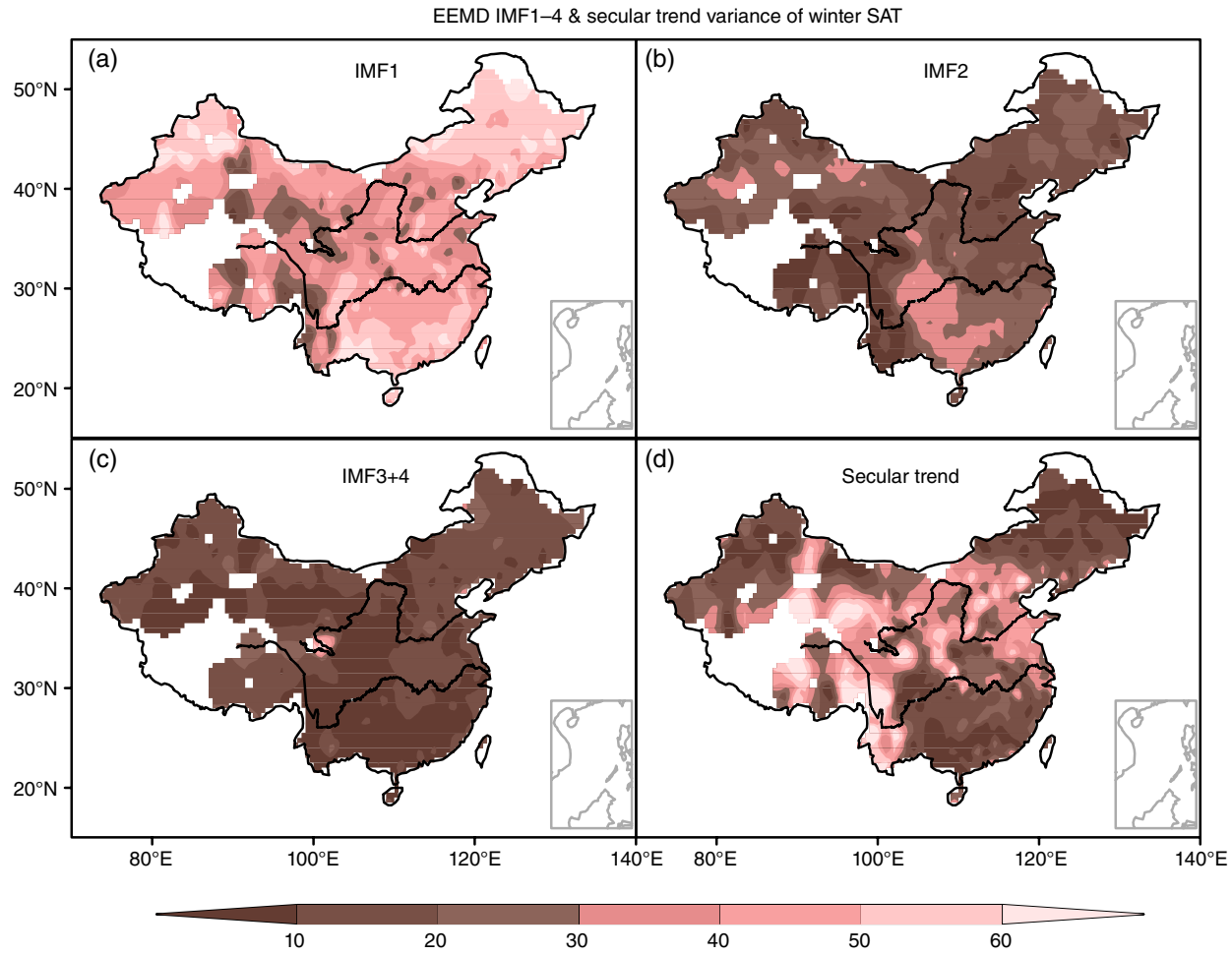

Figure 1. Spatial distribution of variances explained by (a) IMF1, (b) IMF2, (c) IMF3+4 and (d) secular trend derived from EEMD decompositions of winter SAT over China. [Colour figure can be viewed at wileyonlinelibrary.com].

EEMD is a self-adaptive analysis method that decomposes a time series into several oscillatory components on various time scales and a nonlinear secular trend. Specifically, an ensemble size of 1000 and a white noise with amplitude of 0.2 times the standard deviation of the annual SAT series are used to conduct the EEMD. The observed SAT time series (1961–2014) is decomposed into four intrinsic mode functions (IMFs) and a residual secular trend. The cycles of IMF1 and IMF2 are less than 10 years, indicating interannual variability. IMF3 and IMF4 represent decadal to multi-decadal variations. The principal component analysis is used to examine the leading patterns of SAT at interannual time scales. Furthermore, the correlation and linear regression analyses are performed to investigate the relationship between the SAT and the atmospheric circulation and other factors, assessed using the Student's *t*-test or *F*-test.

3. The year-to-year SAT variability

To investigate the contribution of interannual variability on the total variations of winter SAT over China, we first used the EEMD to extract signals of the SAT variations at various time scales. Figure 1 shows the explained variance of each of the IMFs derived from the EEMD decomposition. The cycle of IMF1 is generally less than 3 years, suggesting 2-year cycle SAT variability. The variance of IMF1 is more than 30% over most parts of China and 40% over large parts of China. In particular, the variance is greater than 50% over northeastern China and parts of northwestern and southeastern China (Figure 1(a)). In comparison with the less than 30% variance in the 3–10-year interannual cycle variability and less than 20% variance in the decadal to multi-decadal variation over most parts of China (Figures 1(b) and (c)), the 2-year cycle variability is much more intensive. Furthermore, except some parts over the Tibetan Plateau and northern China, the variance in IMF1 is also much larger than that of the secular trend (Figure 1(d)). In short, for the SAT over China in winter, the 2-year cycle variability is the most intensive among the variations at various time scales. Based on the aforementioned knowledge, we focus on the 2-year cycle variability of winter SAT over China in the following sections.

Figure 2(a) shows the correlation coefficients between EEMD IMF1 and the year-to-year SAT over China in winter. The coefficients over the whole China are larger than 0.7 for 1961–2014, which exceed the 99.9% confidence

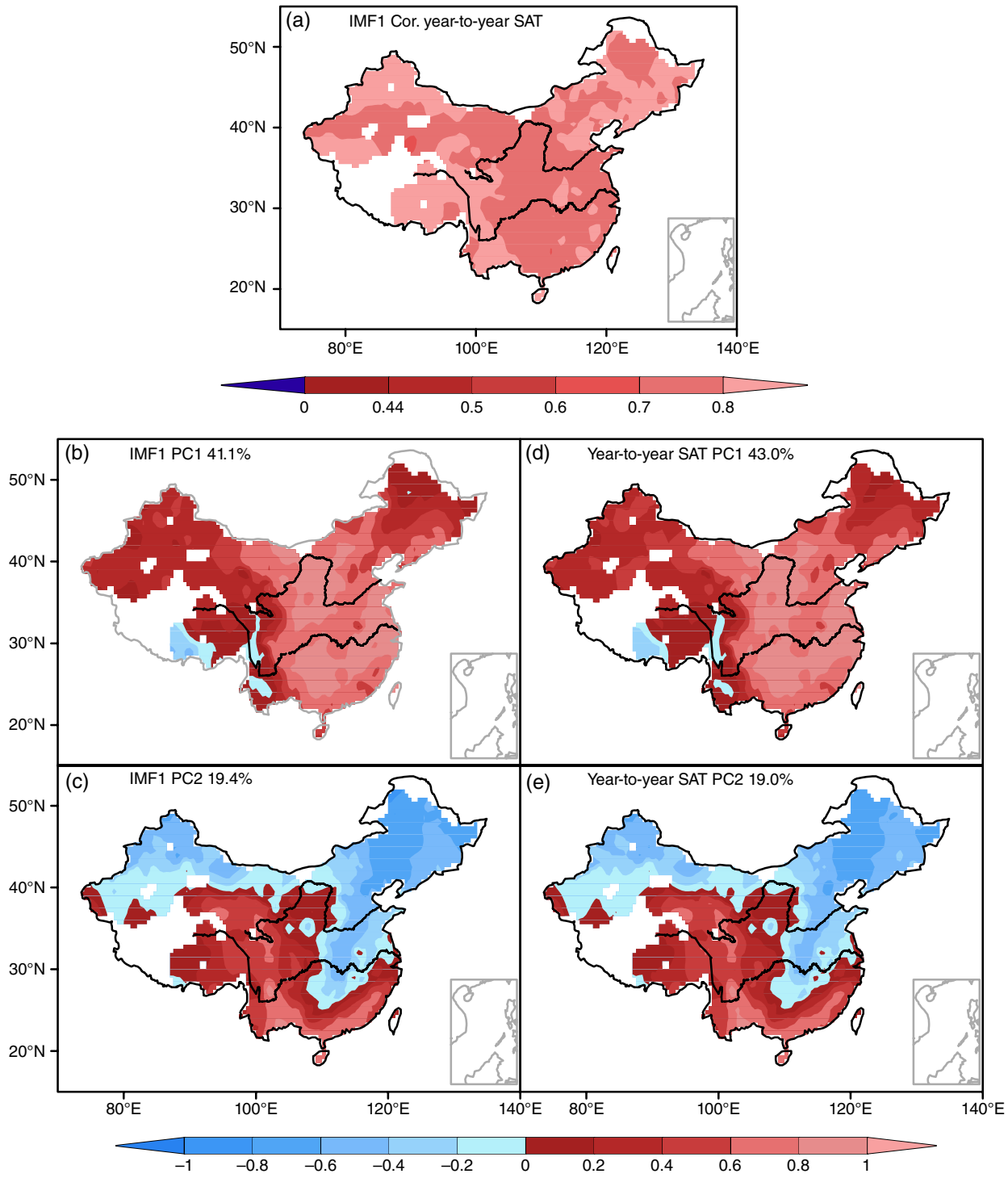

Figure 2. Spatial distribution of the (a) correlation coefficients between IMF1 and year-to-year SAT, and the PC1 mode in terms of (b) IMF1 derived from EEMD decompositions of winter SAT and (d) year-to-year SAT; (c) and (e) are the same as (b) and (d) but for the PC2 modes (unit: K). [Colour figure can be viewed at wileyonlinelibrary.com].

level ($R = 0.44$). Thus, the year-to-year SAT can reflect the exact 2-year cycle variability of the SAT decomposed by the EEMD IMF1. Figures 2(d) and (e) illustrate the first (PC1) and second PCs (PC2) of year-to-year SAT. For the PC1, the year-to-year SAT exhibits a homogeneous variability over most parts of China, except in small areas over the southeastern Tibetan Plateau, with the centre located in eastern China. The PC2 exhibits a south–north dipole, with variability over northern China and the central part of eastern China, opposite from that in southeastern China and on the Tibetan Plateau. Approximately 40% of the variance is explained by the homogeneous variability pattern, and 20% is explained by the south–north dipole pattern. The two leading patterns of IMF1 are quite similar to those of year-to-year SAT (Figures 2(b) and (c)), which further verifies the representativeness of

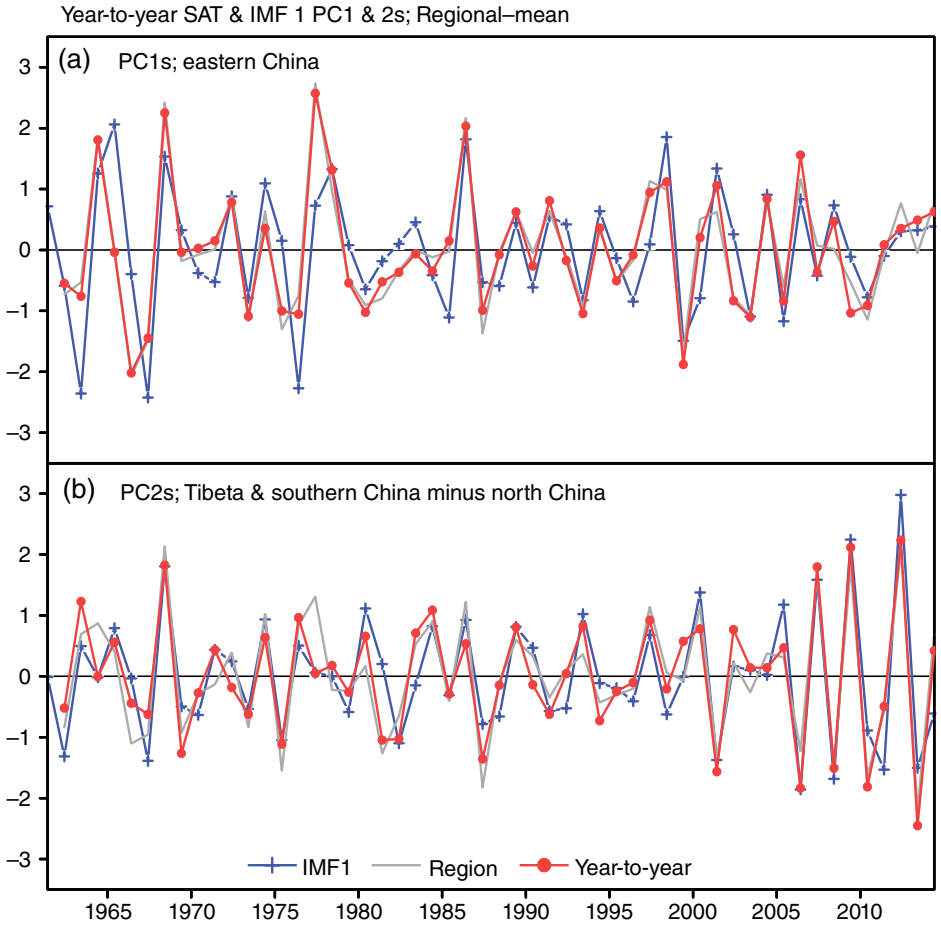

Figure 3. (a) Normalized time series of PC1s in terms of EEMD IMF1 (solid line with cross) and year-to-year winter SAT (solid line with closed cycle) and the year-to-year winter SAT averaged over eastern China (solid line; south of 40°N, 100°–120°E), (b) time series of PC2s in terms of EEMD IMF1 (solid line with cross) and year-to-year winter SAT (solid line with closed cycle) and the difference of year-to-year winter SAT between southern China (south of 26°N), the Tibetan Plateau (south of 40°N, west of 105°E) and northern China (north of 40°N; solid line). [Colour figure can be viewed at wileyonlinelibrary.com].

the year-to-year SAT of the 2-year cycle variability decomposed by the IMF1.

The PC1s of both year-to-year SAT and IMF1 exhibit similar time evolution, with more intensive fluctuation before 1990 than afterwards, suggesting the intensive variability of the homogeneous variability pattern before 1990. Because the centre of the pattern is located in eastern China (south of 40°N, east of 105°E), the time series of the averaged year-to-year SAT over eastern China is also explored in (Figure 3(a)). The correlation coefficient between the PC1 of the year-to-year SAT and the averaged year-to-year SAT over eastern China is 0.97, representing PC1 on behalf of the year-to-year SAT over eastern China. Generally, the PC2 of year-to-year SAT exhibits a weaker fluctuation in comparison with the PC1s before 2005 (Figure 3(b)). That is, the homogeneous variability pattern is more intensive than the south–north dipole pattern before 2005. After 2005, the south–north dipole pattern becomes evident and abrupt, and its variability is more robust than that of the homogeneous variability pattern. The PC2 of IMF1 exhibits similar variability to that of year-to-year SAT. Similarly, because the centres of PC2 are located in southern China, over the Tibetan Plateau and northern China, we calculate the difference in year-to-year SAT averaged over southern China (south of 26°N) and the Tibetan Plateau (south of 40°N, west of 105°E) minus the year-to-year SAT averaged over northern China (north of 40°N). As expected, the difference indicates a quite similar variability with the PC2 of the year-to-year SAT ($R = 0.92$), justifying the PC2 on behalf of the year-to-year SAT over northern China opposite to that over southern China and the Tibetan Plateau.

Figure 4 illustrates the spatial distribution of the correlation coefficients between the PC1 and PC2 of the year-to-year SAT over China and the year-to-year SAT over the global land surface in winter. Except for the significant positive relationship with year-to-year SAT over most of China, there is no significant relationship between PC1 and year-to-year SAT over other regions at a continent scale. In contrast, PC2 exhibits a significantly negative relationship with the year-to-year SAT over large parts of the Eurasian landmass, beside a significant positive relationship with the year-to-year SAT over southern China and the Tibetan Plateau and a significant negative relationship with the year-to-year SAT over northern China. It seems that this homogeneous variability pattern

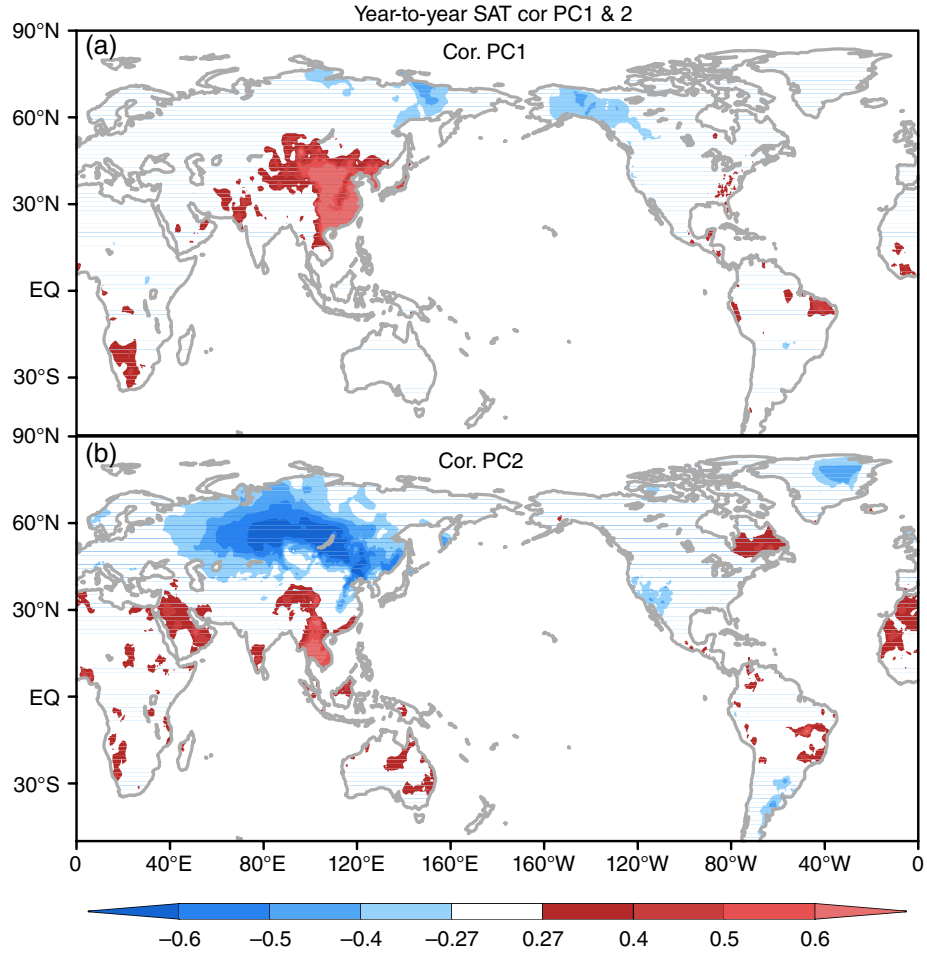

Figure 4. (a) Spatial distribution of the correlation coefficients between the PC1 of year-to-year winter SAT over China and the global year-to-year winter SAT; (b) the same as (a) but for PC2. Shadings denote the correlations exceeding the 95% confidence level. [Colour figure can be viewed at wileyonlinelibrary.com].

is independent of the year-to-year SAT over other regions, whereas the south–north pattern is part of the Eurasian year-to-year SAT at a continental scale.

4. Associated atmospheric circulation

Figures 5(a) and (b) demonstrate the regression of the winter surface level pressure (SLP) and horizontal winds at 850 hPa on PC1 and PC2. PC1 exhibits a significant positive relationship with the anomalous anticyclone over the northern Pacific, whereas PC2 exhibits a significant relationship with the anomalous negative NAO. We further investigate the relationship between year-to-year SLP and horizontal winds at 850 hPa and PC1 and PC2. It seems that the relationship of PC1 to the atmospheric circulation west of 180°E is significant, whereas PC2 exhibits a significant relationship to the atmospheric circulation east of 180°E (Figures 5(c) and (d)). Over the mid- to high latitudes, PC1 is associated with a significantly strengthened AO, which exists only over the Pacific portion, with the Arctic vortex centring southwards to northern Eurasia. In comparison, PC2 is accompanied by a significantly weakened NAO and a north–south dipole over the northern Pacific. In tropical and subtropical zones, PC1 exhibits a significant positive relationship with SLP over the Indian Ocean and western Pacific, whereas PC2 exhibited a significant negative relationship with SLP over the central and eastern Pacific. In China, PC1 is associated with significant positive SLP anomalies over western China, but negative SLP anomalies over eastern China. PC2 is accompanied by significant positive SLP anomalies over northern China, whereas negative SLP anomalies over southern China and the Tibetan Plateau. Except for the significant southerly flow over southern China, there is no obvious low-level meridional wind anomaly associated with PC1 or PC2 over China.

In the mid- to high-level troposphere, PC1 corresponds to an anomalous anticyclone over the midlatitude zone from Eurasia eastwards to the Pacific and an anomalous cyclone over northern Eurasia and the polar zone, with the positive anomalies centred in the northern Pacific and negative anomalies centred over eastern Siberia (Figures 6(a) and (c)). It seems that positive AO anomalies only exist over the eastern part and a positive centre exists over the Pacific. These positive Pacific-AO anomalies correspond to an anomalous strengthened westerly from Siberia to the northern Pacific, which blocks the cold flows from

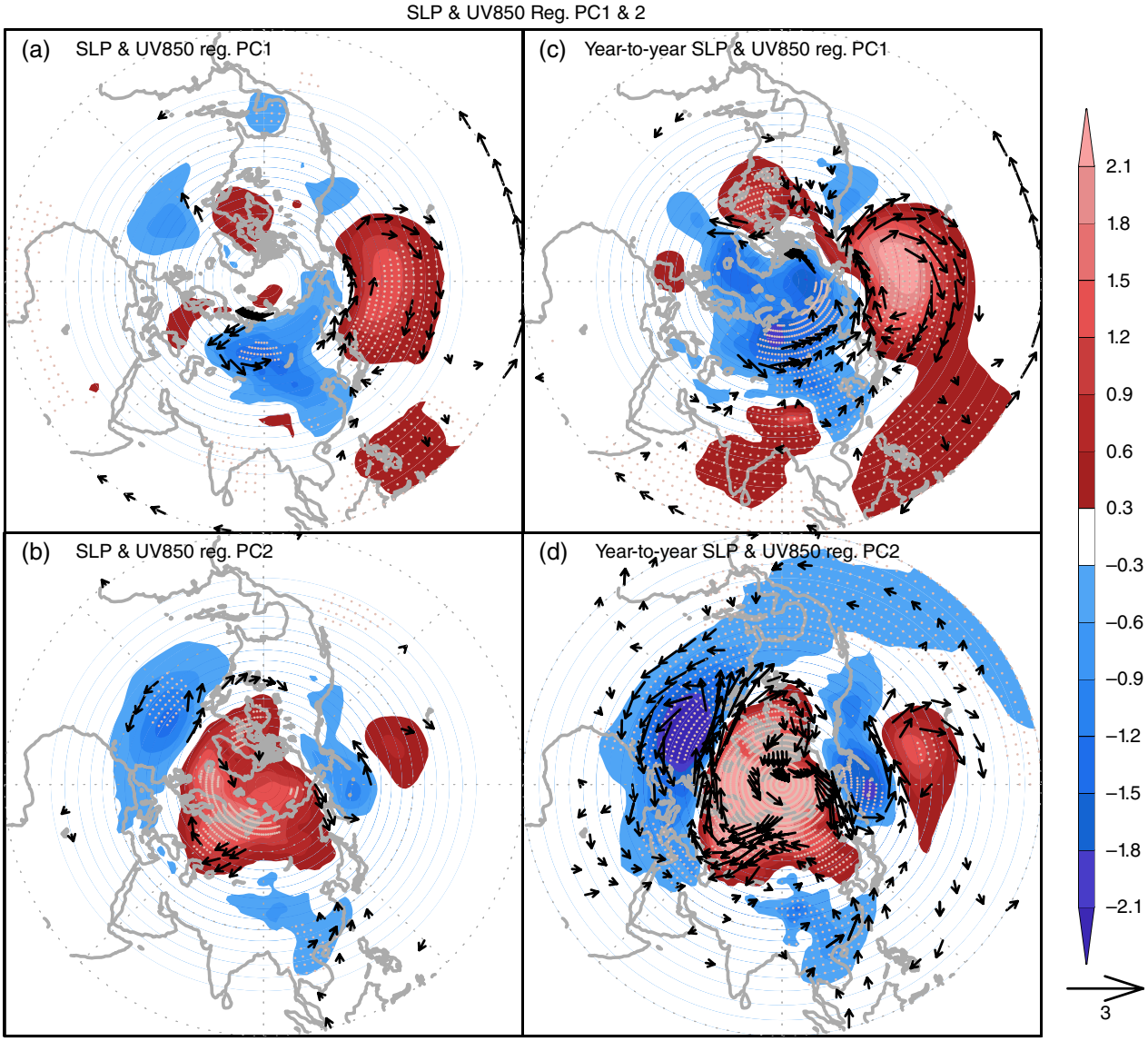

Figure 5. SLP (shaded, Pa) and horizontal winds (vector, m s^{-1}) at 850 hPa in winter regressed on (a) the PC1 and (b) PC2 of year-to-year winter SAT over China; (c) and (d) are same as (a) and (b) but for the year-to-year sea level pressure and horizontal winds at 850 hPa in winter. The dots denote the sea level pressure anomalies exceeding the 95% confidence level, and horizontal wind anomalies exceeding the 95% confidence level are drawn. [Colour figure can be viewed at wileyonlinelibrary.com].

the polar area southwards to China. Consequently, the abnormal warm easterly flow from the Pacific dominates China (Figures 6(a) and (c)). That is, positive Pacific-AO anomalies with a southwards Arctic vortex centre and a strengthened and southwards west jet stream are significantly related to the homogeneous warmth pattern over China. The mid- to high-level tropospheric atmospheric circulation anomalies associated with PC2 are much more intensive than those associated with the PC1 (Figures 6(b) and (d)). Accompanied by the south–north dipole, the atmospheric circulation exhibits significantly negative AO anomalies over the mid- to high latitudes, with two negative centres over Siberia and the northern Atlantic. The cold airflow derived from the weakened polar vortex intrudes southwards, converging with the anomalous westerly flow due to the anomalous cyclones over Siberia, corresponding to the anomalous northwesterly flow over northern China. An anomalous anticyclonic circulation occurs around southern China in the mid-level troposphere, suggesting the dominance of anomalous southeasterly movement over southern China. Focusing on China, a weakened SLP with a strengthened geopotential height in the mid- to high-level troposphere occurring over eastern China is associated with PC1. That is, an anomalous descending movement over eastern China is associated with the homogeneous warm pattern. For the south–north dipole pattern, the SLP strengthened, whereas the geopotential height in the mid- to high-level troposphere weakened over northern China, indicating anomalous ascent dominating the vertical circulation over northern China. The weakened SLP and strengthened geopotential height in the mid- to high-level troposphere over southern China are suggestive of descending movement over southern China.

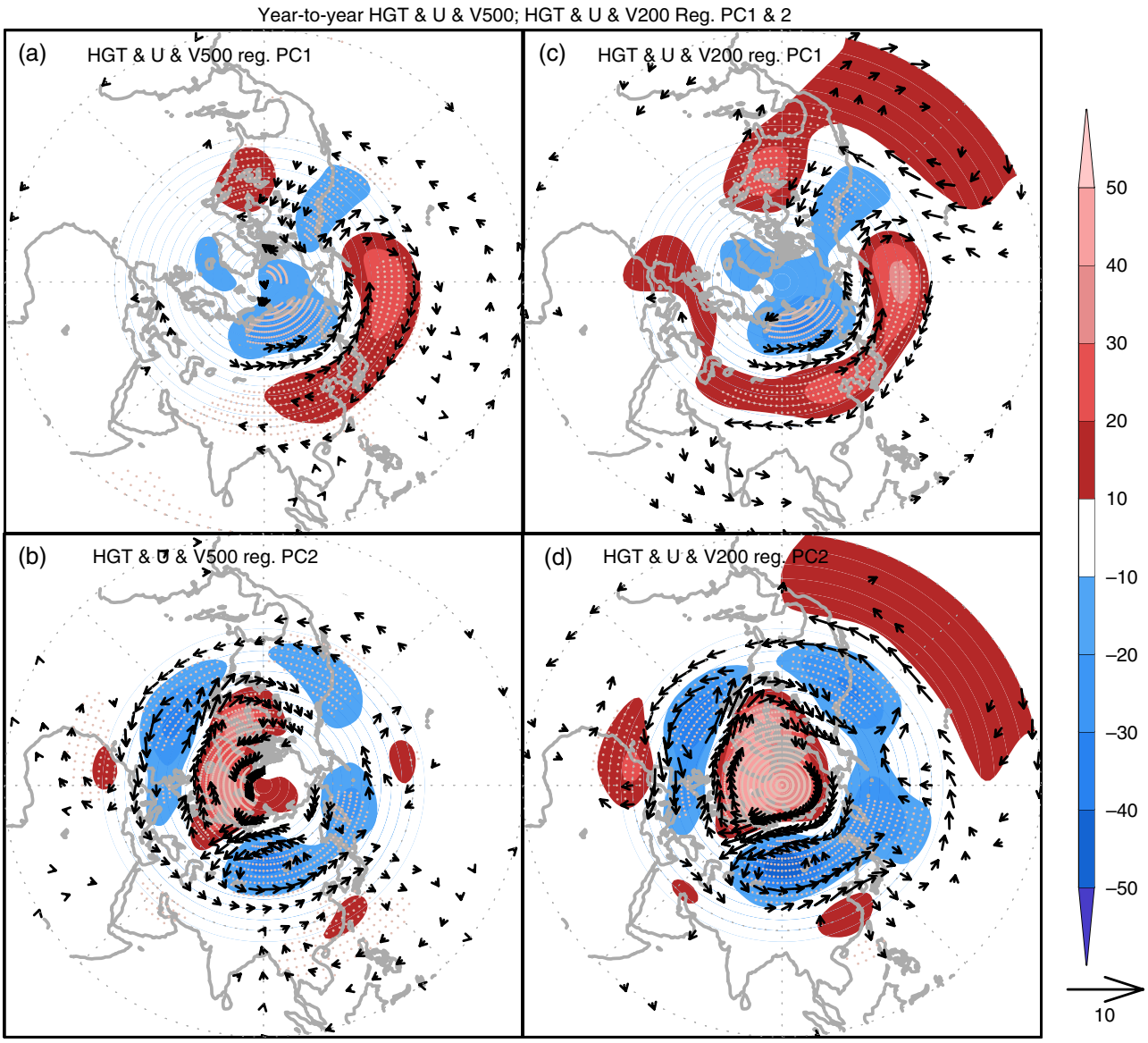

Figure 6. Year-to-year geopotential height (shaded, gpm) and horizontal winds (vector, m s^{-1}) at 500 hPa in winter regressed on (a) the PC1 and (b) PC2 of year-to-year winter SAT over China; (c) and (d) are the same as (a) and (b) but for 200 hPa. The dots denote the sea level pressure anomalies exceeding the 95% confidence level, and the horizontal wind anomalies exceeding the 95% confidence level are drawn. [Colour figure can be viewed at wileyonlinelibrary.com].

It is likely that PC1 is a response to the anomalies at a regional scale, whereas PC2 is a response to the anomalies at a hemispheric scale. The homogeneous variability pattern is only significantly related to the Pacific-AO, whereas the south–north dipole pattern is significantly related to the AO. The variance in PC1 is twofold larger than that of PC2, suggesting the more important impacts of the Pacific-AO compared to the impacts of the AO on the SAT over China. Furthermore, the magnitude of the anomalous geopotential height associated with PC2 is much larger in comparison with PC1, with an absolute value larger than 40 gpm over the positive and negative centres, which is generally more than twice that of the anomalies associated with PC1. Even for SLP, the anomalies associated with PC1 are also generally weaker than those associated with PC2 (Figure 5). In other words, a moderate Pacific-AO anomaly may be enough for the occurrence of a homogeneous variability pattern, whereas an intensive AO anomaly is essential to the occurrence of the south–north dipole pattern.

5. Plausible causes

5.1. Sea surface temperature

Figures 7(a) and (b) illustrate the regression of year-to-year SST on PC1 and PC2 in the previous winter (December–January–February), spring (March–April–May), summer (June–July–August) and autumn (September–October–November) and in the current winter and spring. For both PC1 and PC2, there are no significant relationships to the SST over the tropical

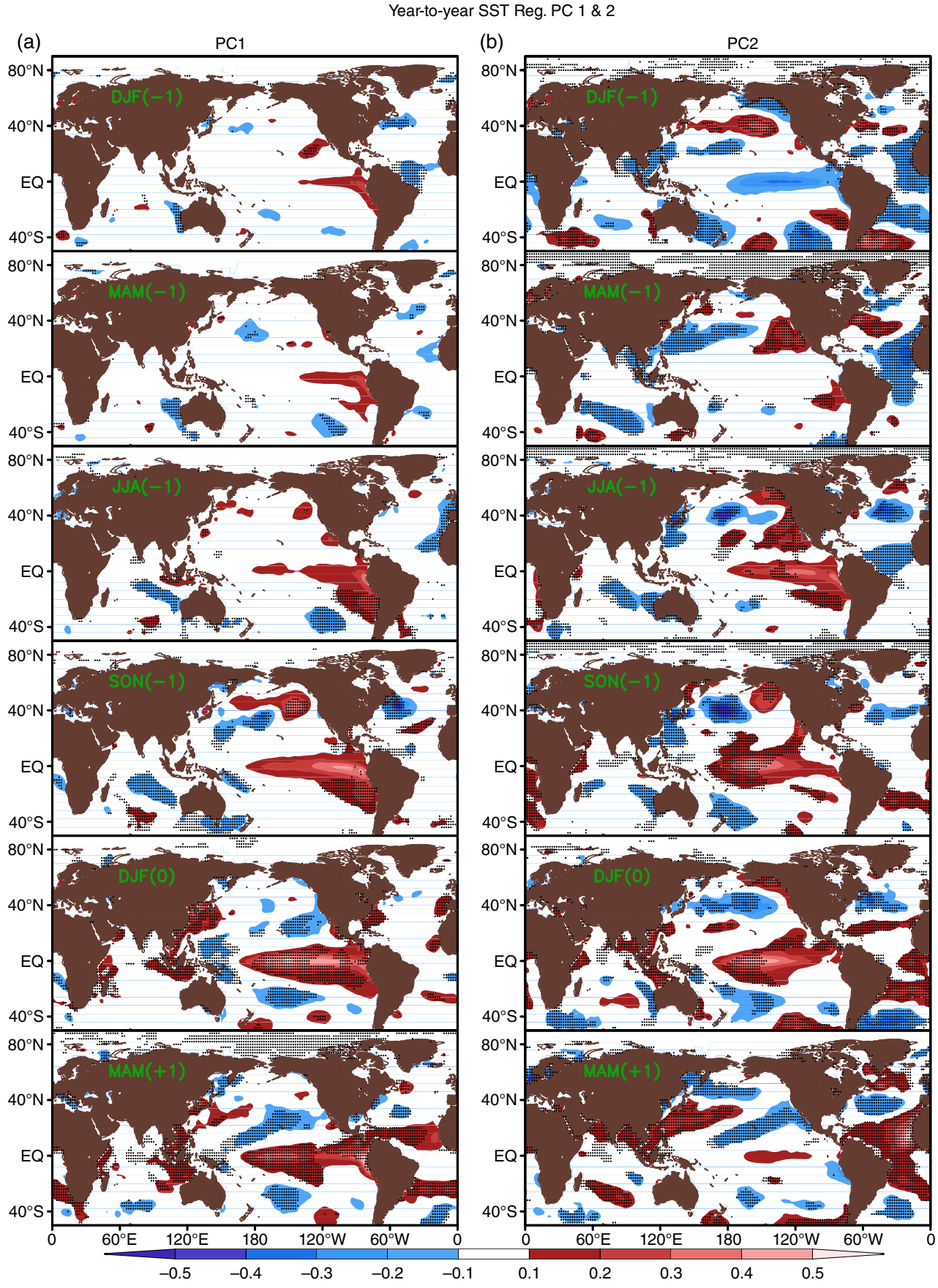

Figure 7. Year-to-year SST (shaded, K) in the previous winter, spring, summer, autumn, and the current winter and following spring regressed on (a) the PC1 and (b) PC2 of year-to-year winter SAT over China. The dots denote the sea level pressure anomaly exceeding the 95% confidence level. [Colour figure can be viewed at wileyonlinelibrary.com].

Pacific in the previous winter and spring, suggesting that the leading two patterns are not related to the previous El Niño. In the previous summer, the PC1 is associated with significantly positive SST anomalies that occurred over the southeastern subtropical Pacific, which become more significant in the previous autumn. Furthermore, there is a positive Indian Ocean dipole anomaly associated with the PC1 in the previous autumn. The positive SST anomalies over the subtropical southern Pacific and the positive Indian Ocean dipole anomaly in the previous autumn influence the development of El Niño in the current winter and the following spring through an anomalous westerly wind and the modulation of the strength of the walk circulation in the autumn, respectively (Izumo *et al.,* 2010; Min *et al.,* 2015); this may have contributed to the significant relationship between El Niño and PC1 in the current winter and following spring. Overall, the anomalous significant SST over the southeastern subtropical Pacific and Indian Ocean dipole in the previous autumn play a key role in the homogeneous variability pattern by inducing the development of El Niño. PC2 exhibits a significant relationship with the SST over the Atlantic and Arctic Oceans in the previous winter, spring and summer. However, the significant relationship of PC2 with the Atlantic SST disappeared, whereas a significant positive SST anomaly over the central tropical and subtropical Pacific occurs in the previous autumn, resembling a type of central Pacific El Niño. The central Pacific type of El Niño becomes weak in the current winter and disappears in the following spring. At the same time, the relationship of PC2 to the Atlantic SST becomes significant in the current winter and more obvious in the following spring. It seems that the change in the relationship of PC2 to the Atlantic SST is due to the seasonal oscillation of the Atlantic SST or due to a response to certain forcing. The central Pacific-type El Niño in the previous autumn may be the key factor of the south–north dipole pattern.

Because of the significant impact of the autumn SST over the three key regions, we further investigate two regions, including the subtropical southeastern Pacific (25°–10°S, 100°–75°W) and the Indian Ocean dipole (50°–30°S, 70°–90°E minus 25°–5°S, 80°–100°E), for PC1 and the tropical central Pacific (15°S–15°N, 170°E–150°W) for PC2, and their relationship to the year-to-year SAT over China in winter (Figure 8). As expected, the Indian Ocean dipole anomaly is generally associated with the homogeneous variability pattern, except for small parts over northeastern and northwestern China (Figure 8(a)). The regression of year-to-year SAT is significant over most parts of eastern China, where the variability is most intensive in the homogeneous variability pattern. In comparison, although the subtropical southern Pacific SST anomaly corresponds to the anomalous positive year-to-year SAT over eastern China, significant regression of year-to-year SAT is mainly located in the area between 100° and 105°E and southeastern China (Figure 8(b)). Furthermore, there are obvious negative anomalies over parts of northeastern and northwestern China. Clearly, compared to the SST

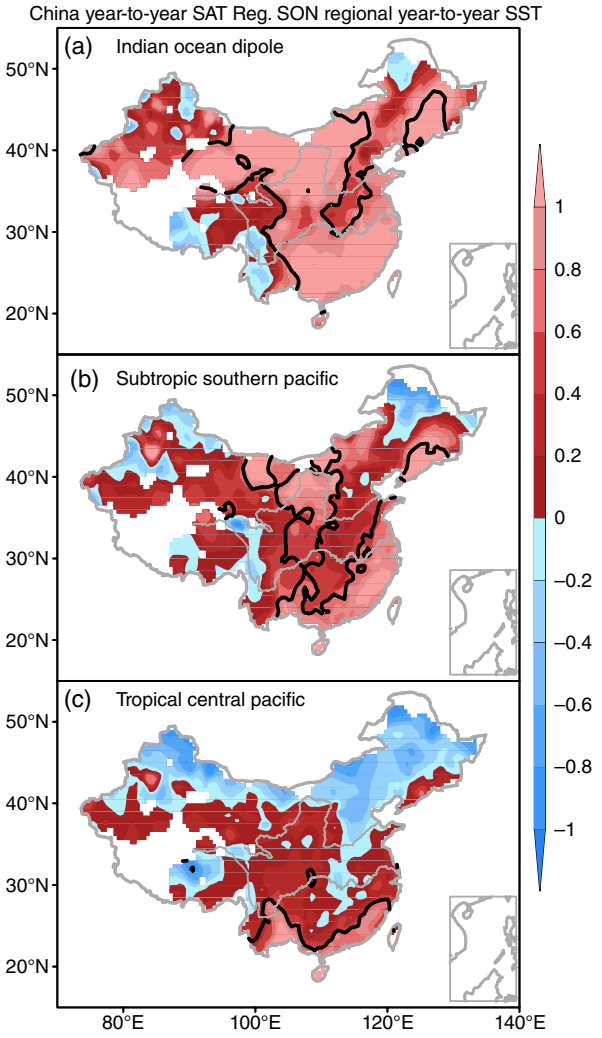

Figure 8. Year-to-year winter SAT over China (K K^{-1}) regressed on (a) year-to-year Indian Ocean dipole SST (50°–30°S, 70°–90°E minus 25°–5°S, 80°–100°E), (b) year-to-year SST over the subtropical southern Pacific (25°–10°S, 100°–75°W) and (c) year-to-year SST over the tropical central Pacific (15°S–15°N, 170°E–150°W) in previous autumn. The lines denote regression exceeding the 95% confidence level. [Colour figure can be viewed at wileyonlinelibrary.com].

over the subtropical southern Pacific, the Indian Ocean dipole plays a more important role in the homogeneous variability pattern. In fact, an Indian Ocean dipole in a previous autumn can trigger a Pacific-AO circulation anomaly in the winter at 500 hPa, which is more similar to the Pacific-AO circulation than that associated with PC1 (figure not shown). Figure 8(c) shows the regression of year-to-year SAT on year-to-year SST over the tropical central Pacific. Although the SST over the tropical central Pacific is associated with a south–north dipole pattern, the regression of year-to-year SAT over most parts of China does not exceed the 95% confidence level, except in southeastern China. The central-type El Niño may only play a significant role on the year-to-year SAT over southeastern China. Overall, in comparison with the homogeneous variability pattern, the impact of SST on the south–north dipole pattern is much weaker. Namely, other factors, such as snow cover and sea ice which have

been reported by previous studies (Wang *et al.,* 2010a; Wang *et al.,* 2010b; Sun *et al.,* 2016), may play a more important role in the south–north dipole pattern.

5.2. Sea ice and snow cover

Figure 9 shows the regression of year-to-year sea ice concentration in the previous September on PC1 and PC2. Generally, PC1 does not exhibit a significant relationship with sea ice concentration at a regional scale (Figure 9(a)). In comparison, the sea ice concentration over large parts of north of 65°N Arctic, especially over the Sea of Okhotsk, exhibits a significant negative relation to PC2 (Figure 9(b)). The reduced sea ice over the Arctic provides favourable conditions for the intrusion of cold air to northern East Asia by reducing the meridional thickness gradient between the middle and high latitudes (Sun *et al.,* 2016). Figure 9(d) demonstrates the significant positive relationship between the PC2 and the year-to-year snow cover fraction over large parts of Eurasia in the previous November, which justifies previous studies where the loss of sea ice anomaly generally corresponds to anomalous extensive snow cover over Eurasia and then a cold Eurasian continent (Honda *et al.,* 2009; Mori *et al.,* 2014). In comparison, PC1 is significantly negatively related to the snow cover fraction around China in the previous November (Figure 9(c)). The homogeneous warmth over China may be a consequence of less snow cover around China in the previous November, not remotely related to the snow cover or sea ice anomalies over high latitudes.

Figure 10(a) illustrates the regression of the year-to-year SAT over China on the year-to-year snow cover fraction around China (40°–50°N, 80°–140°E) in November. The homogeneous negative anomalies, except parts of northwestern China and the Tibetan Plateau, are associated with the snow cover fraction around China, with the anomaly exceeding the 95% confidence level over most of eastern China. This indicates less snow cover around China in November and more warmth throughout China in the winter. As Sun *et al.* (2016) have reported the impact of Barents–Laptev sea ice concentration on the SAT over East Asia in the winter, we focus here on the impact of sea ice concentration over the Okhotsk Sea (45°–60°N, 140°–150°E). The Okhotsk sea ice concentration in September exhibits a significant positive relationship

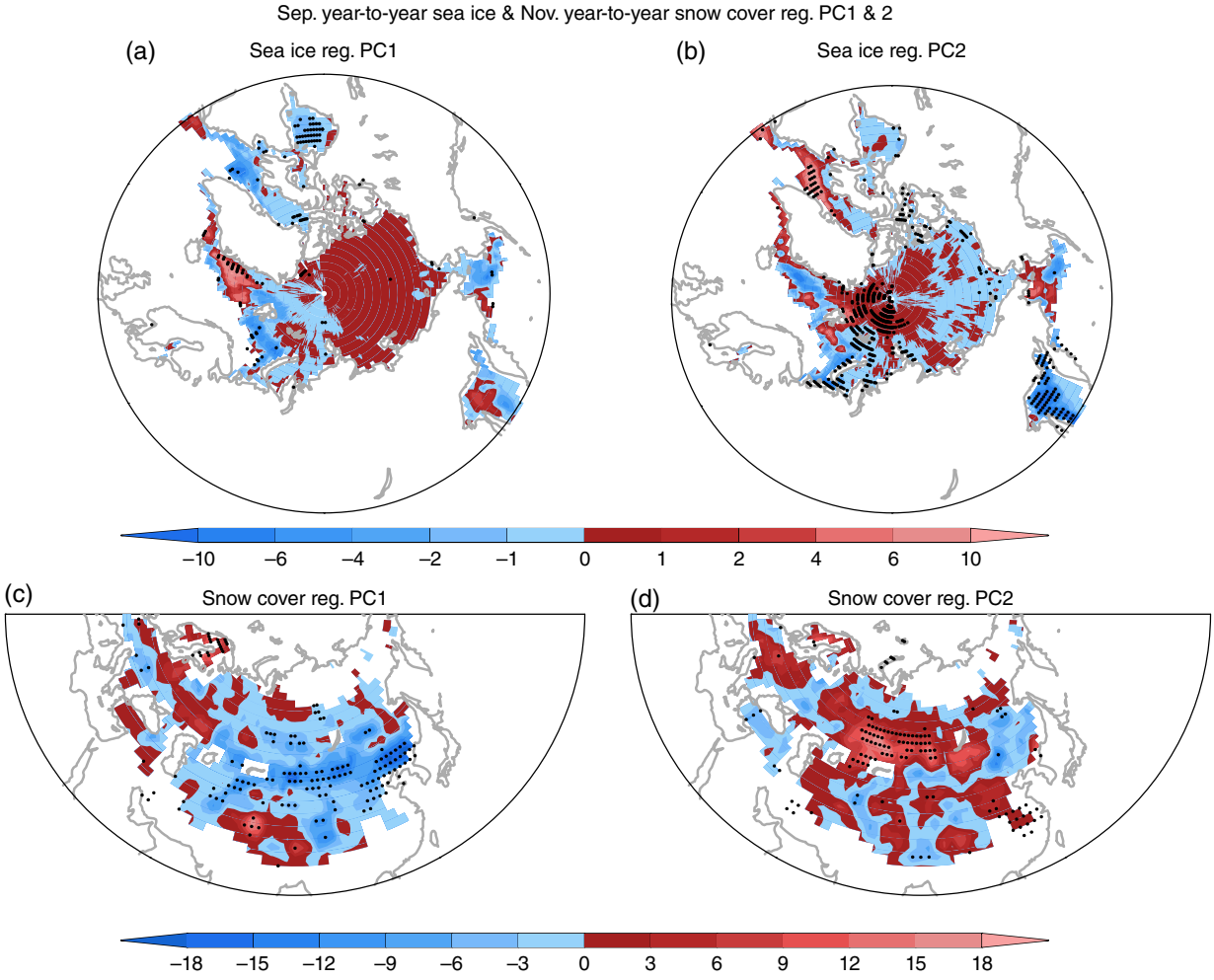

Figure 9. Year-to-year sea ice concentration in the previous September (unit: %) regressed on (a) the PC1 and (b) PC2 of year-to-year winter SAT over China; (c) and (d) are the same as (a) and (b) but for the year-to-year snow cover fraction (unit: %) in the previous November during 1966–2009. The dots denote regressions exceeding the 95% confidence level. [Colour figure can be viewed at wileyonlinelibrary.com].

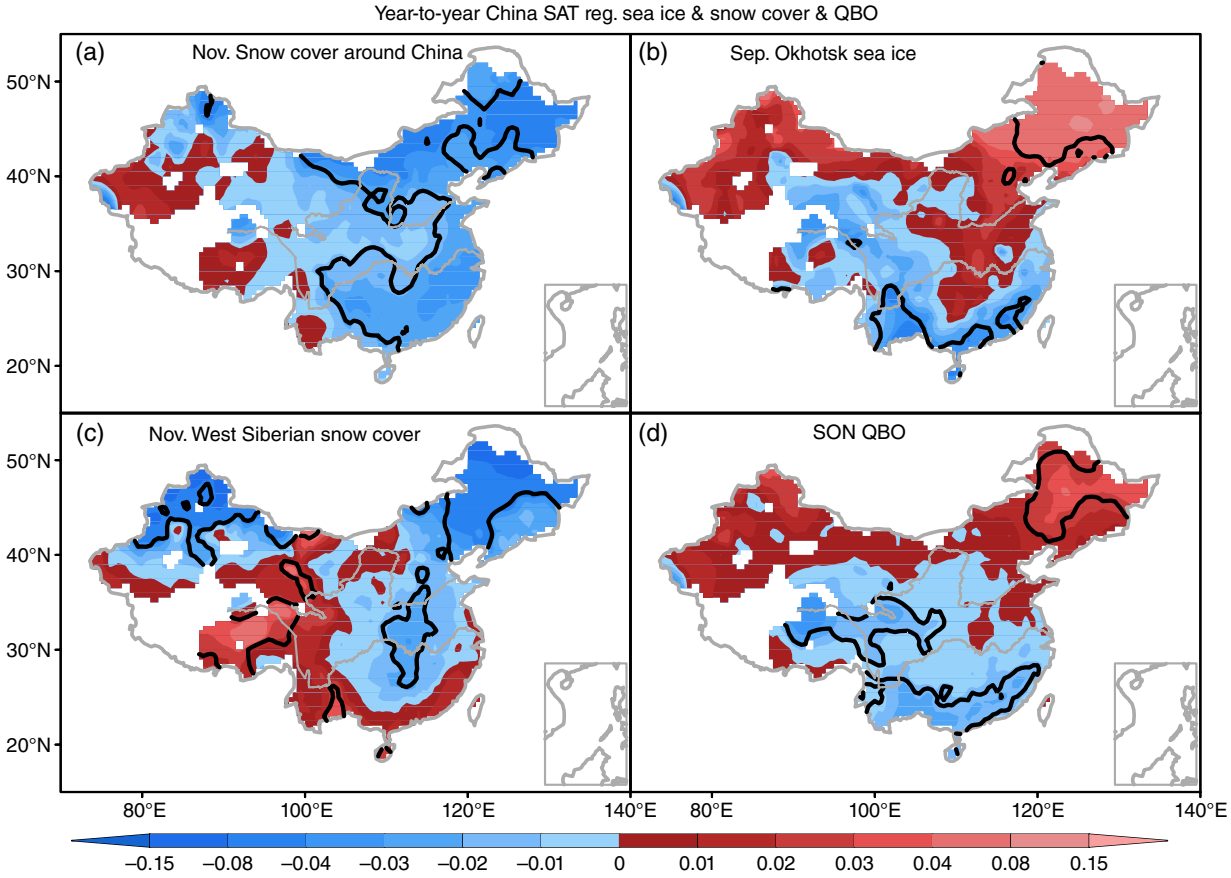

Figure 10. Year-to-year winter SAT over China regressed on (a) year-to-year snow cover fraction around China and (c) western Siberia in the previous November during 1966–2009, (b) sea ice concentration around the Sea of Okhotsk (25°–10°S, 100°–75°W) in the previous September (unit: K %$^{-1}$) and (d) stratospheric QBO in the previous autumn (unit: K s m^{-1}). The lines denote regressions exceeding the 95% confidence level. [Colour figure can be viewed at wileyonlinelibrary.com].

to the year-to-year SAT over northeastern China and a significant negative relationship to the year-to-year SAT over southeastern China (Figure 10(b)). The snow cover fraction over western Siberia (50°–60°N, 60°–80°E) in November indicates a significant negative relationship to the year-to-year SAT over northeastern and northwestern China and over central eastern China and a significant relationship to the year-to-year SAT over the Tibetan Plateau (Figure 10(d)). Furthermore, both the regression of year-to-year SAT on Okhotsk sea ice concentration and on the snow cover fraction over western Siberia exhibits a south–north dipole anomaly, which is similar to the south–north dipole pattern disclosed by the PC2 mode.

The Indian Ocean dipole in the previous autumn and the snow cover fraction around China in November are the two key factors of the homogeneous variability pattern. That is, the positive Indian Ocean dipole in the previous autumn and less snow cover fraction throughout China in November are associated with a warm winter over China. Because the homogeneous variability pattern explains more than 40% of the variance, these two factors are clearly important for in climate prediction. In comparison, the factors on the south–north dipole pattern are relatively complicated. The pattern is part of the year-to-year SAT at a continental scale, and thus this pattern is likely the consequence of the joint effect of a central-type El Niño and the sea ice and snow cover, with the central-type El Niño contributing to the year-to-year SAT anomalies over southeastern China, and the sea ice and snow cover over Siberia contributing to the year-to-year SAT anomalies over northern China and the Tibetan Plateau. Namely, less sea ice over high latitudes and of Okhotsk Sea in September, and more snow cover over western Siberia and central-type El Niño anomalies in autumn correspond to cold winter over northern China and central eastern China and warm winter over southeastern China and on the Tibetan Plateau.

5.3. Other factors

Previous studies have also suggested an impact of stratospheric QBO on the SAT variability over China (Li and Long, 1992). Figure 10(d) illustrates the regression of year-to-year SAT over China on the year-to-year stratospheric QBO in the previous autumn. The year-to-year SAT anomalies over China are similar to the south–north dipole pattern, with a correlation coefficient between QBO and PC2 exceeding the 99% confidence level. A positive QBO anomaly is associated with a significant warmth anomaly over northeastern China and a significant cold anomaly over southeastern China and the Tibetan Plateau in winter. Douville *et al.* (2017) reported

that the QBO is partly responsible for the relationship between Siberian snow cover and the SAT over Eurasian landmasses in winter. Furthermore, Li *et al.* (2011) found that a strong (weak) East Asian summer monsoon is generally associated with a weak (strong) EAWM; we also investigate the relationship of the East Asian summer monsoon to the year-to-year SAT over China in winter. Although the East Asian summer monsoon exhibits a significant relationship with the year-to-year SAT over southeastern China (figure not shown), it does did not show a significant relation to the PC1 or PC2.

6. Summary and conclusion

Previous studies have investigated the leading patterns of SAT during the East Asian winter and the possible causes of variability at interannual and decadal time scales (Wang *et al.,* 2010a; Wang *et al.,* 2010b; Sun *et al.,* 2016). This study focused on the two leading patterns of year-to-year SAT over China in winter and the plausible causes, because the year-to-year variability contributes to the most variance at various time scales. Furthermore, because the prediction of winter SAT over China is one of the most important elements for climate prediction at the Chinese Meteorological Administration, we need to investigate the leading patterns of SAT over China in detail.

The two leading patterns of year-to-year SAT over China in winter explain over 60% of the variance. The first pattern shows homogeneous variability across China, with the centre located south of 40°N in eastern China. This pattern does not show a significant relationship with the SAT over most parts of the global landmass, even for the SAT during the EAWM domain beside China. The second pattern exhibits a south–north dipole, with the variability over northern China that was opposite to that over southeastern China and the Tibetan Plateau. In contrast to the homogeneous variability pattern, the south–north dipole pattern is significantly related to the SAT over large parts north of 50°N on the Eurasian landmass. Namely, the homogeneous variability pattern is independent of the SAT over other regions, whereas the south–north dipole pattern is part of the global SAT variability. It is important to note that the first pattern explains more than 40% of the variance, and we need to investigate the pattern of SAT over China alone and not only treat it as one part of the SAT in the EAWM domain.

The most evident atmospheric circulation anomaly associated with the homogeneous variability pattern is located in the northern Pacific. When the homogeneous variability pattern is in a positive phase, the SLP exhibits an anomalous significant anti-cyclone around the northern Pacific and an anomalous cyclone around eastern Siberia, resembling a type of positive Pacific-AO. This positive Pacific-AO also exists in the mid- to top-level troposphere, with an anomalous anti-cyclone occurring around the northern Pacific and extending westwards to midlatitude Eurasia. The westerly jet stream is strengthened and moves northwards, and the anomalous easterly air flow from the warm ocean dominates China. Consequently, the SAT exhibits a significant warmth anomaly throughout China. The circulation anomaly associated with the south–north dipole pattern is quite different from that with the homogeneous variability pattern. The south-warm/north-cold pattern is related to a significant negative NAO in the low-level troposphere and a significant negative AO in the mid- to top-level troposphere. The anomalous northwesterly airflow may contribute to the cold over northern China. In comparison, the atmospheric circulation anomalies associated with the homogeneous variability pattern are much weaker than those with the south–north dipole pattern, suggesting that a moderate circulation anomaly can trigger a homogeneous variability pattern, whereas a sufficient intensive circulation anomaly can correspond to a south–north dipole pattern. This phenomenon may be the consequence of that the south–north dipole pattern is part of the continental SAT anomalies, whereas the SAT anomaly disclosed by a homogeneous variability pattern only occurs over China. Furthermore, the phenomenon may also be the reason that the homogeneous variability pattern explains more than twice the variance of the south–north dipole pattern.

The Indian Ocean dipole and the snow cover around China are two key causes of the homogeneous variability pattern. The positive (negative) Indian Ocean dipole in the previous autumn and less (more) snow cover around China in November accompanies warmth (cold) in China during the winter. In comparison, the causes of the south–north dipole pattern are much more complicated. Although the SST over the tropical central Pacific and stratospheric QBO in the previous autumn, Okhotsk sea ice in September and the snow cover over western Siberia in November are significantly related to the south–north dipole pattern, the impacts of these factors are quite different. The SST over the tropical central Pacific, representing a central-type El Niño, only exhibits significant influence on the SAT over southeastern China. The positive stratospheric QBO and Okhotsk sea ice anomalies correspond to significant anomalous warmth in northern China and cold in southeastern China. More snow cover over western Siberia is associated with anomalous cold in northern China and in the central part of eastern China along with anomalous warmth on the Tibetan Plateau. Therefore, the south–north dipole pattern is the consequence of joint effects of the above factors. Based on the above, it is clear that the impact of the tropical Pacific SST on the SAT over China in the winter is not as great as we expected, and further study of the SST over the Indian Ocean is required.

Acknowledgements

This study was jointly supported by the National Key Research and Development Program (2016YFA0601502), the National Natural Science Foundation of China (41375092, 41221064 and 41405078) and by the Basic

Research Fund of the Chinese Academy of Meteorological Sciences (2015Z001).

References

Barnes EA. 2013. Revisiting the evidence linking Arctic amplification to extreme weather in midlatitudes. *Geophys. Res. Lett.* **40**: 4728–4733.

Budikova D. 2009. Role of Artic sea ice in global atmospheric circulation: a review. *Global Planet. Change* **68**: 149–163.

Chang CP, Li T. 2000. A theory for the tropical tropospheric biennial oscillation. *J. Atmos. Sci.* **57**(14): 2210–2224.

Chen W, Li T. 2007. Modulation of Northern Hemisphere wintertime stationary planetary wave activity: East Asian climate relationships by the quasi-biennial oscillation. *J. Geophys. Res.* **112**: D20120. https://doi.org/1029/2007JD008611.

Douville H, Peings Y, Saint-Martin D. 2017. Snow-(N)AO relationship revisited over the whole twentieth century. *Geophys. Res. Lett*. **44**: 569–577.

Fan K. 2009. Predicting winter surface air temperature in Northeast China. *Atmos. Oceanic Sci. Lett.* **2**: 14–17.

Francis JA, Vavrus SJ. 2012. Evidence linking Arctic amplification to extreme weather in mid-latitudes. *Geophys. Res. Lett.* **39**: L06801.

Gao H, Yang S. 2009. A severe drought event in northern China in winter 2008-09 and the possible influences of La Nina and Tibetan Plateau. *J. Geophys. Res.* **114**: D24104.

Gao YQ, Sun JQ, Li F, He SP, Sandven S, Yan Q, Zhang ZS, Lohmann K, Keenlyside N, Furevik T, Suo LL. 2015. Arctic sea ice and Eurasian climate: A review. *Adv. Atmos. Sci.* **32**: 92–114.

Gong DY, Wang SW, Zhu JH. 2001. East Asian winter monsoon and Arctic oscillation. *Geophys. Res. Lett.* **28**: 2073–2076.

He SP, Wang HJ. 2013. Impact of the November/December Arctic Oscillation on the following January temperature in East Asia. *J. Geophys. Res. Atmos.* **118**: 12981–12998.

He SP, Gao YQ, Li F, Wang HJ, He YC. 2017. Impact of Arctic Oscillation on the East Asian climate: a review. *Earth Sci. Rev.* **164**: 48–62.

Honda M, Inoue J, Yamane S. 2009. Influence of low Arctic sea-ice minima on anomalously cold Eurasian winters. *Geophys. Res. Lett.* **36**: L08707. https://doi.org/10.1029/2008GL037079.

Huang F, Gao C-H. 2012. Interannual variations of winter temperature in East Asia and their relationship with sea surface temperature and sea ice concentration (in Chinese). *Period. Ocean Univ. China* **42**: 7–14.

Izumo T, Vialard J, Lengaigne M, Montegut CB, Behera SK, Luo J-J, Cravatte S, Masson S, Yamagata T. 2010. Influence of the state of the Indian Ocean dipole on the following years' El Niño. *Nat. Geosci.* **3**: 168–172.

Kalnay EM, Kanamitsu M, Kistler R, Collins W, Deaven D, Gandin L, Iredell M, Saha S, White G, Woollen J, Zhu Y, Chelliah M, Ebisuzaki W, Higgns W, Janowiak J, Mo KC, Ropelewski C, Wang J, Leetmaa A, Reynolds R, Jenne R, Joseph D. 1996. The NCEP/NCAR 40-year reanalysis project. *Bull. Am. Meteorol. Soc.* **77**: 437–471.

Kang LH, Chen W, Wang L, Chen LJ. 2009. Interannual variations of winter temperature in China and their relationship with atmospheric circulation and sea surface temperature (in Chinese). *Clim. Environ. Res.* **14**: 45–53.

Li C, Long ZX. 1992. QBO and its influence on the general atmospheric circulation and the climate in East China (in Chinese). *J. Atmos. Sci.* **16**: 167–176.

Li F, Wang HJ. 2013. Autumn sea ice cover, winter Northern Hemisphere annular mode, and winter precipitation in Eurasia. *J. Clim.* **26**: 3968–3981.

Li JP, Zeng QC. 2002. A unified monsoon index. *Geophys. Res. Lett.* **29**(8): 1274. https://doi.org/10.1029/2001GL013874.

Li JP, Zeng QC. 2003. A new monsoon index and the geographical distribution of the global monsoons. *Adv. Atmos. Sci.* **20**: 299–302.

Li JP, Zeng QC. 2005. A new monsoon index, its interannual variability and relation with monsoon precipitation. *Clim. Environ. Res.* **10**(3): 351–365.

Li CY, Pan J, Que ZP. 2011. Variation of the East Asian monsoon and the tropospheric biennial oscillation. *Chin. Sci. Bull.* **56**: 70–75.

Liu J, Curry J, Wang H, Song M, Horton R. 2012. Impact of declining Arctic sea ice on winter snowfall. *Proc. Nat. Acad. Sci. USA*. **109**: 4074–4079.

Min QY, Su JZ, Zhang RH, Rong XY. 2015. What hindered the El Niño pattern in 2014? *Geophys. Res. Lett.* **42**: 6762–6770. https://doi.org/1002/2015GL064899.

Mori M, Watanabe M, Shiogama H, Inoue J, Kimoto M. 2014. Robust Arctic sea-ice influence on the frequent Eurasian cold winters in past decades. *Nat. Geosci.* **7**: 869–878. https://doi.org/10.1038/ngeo2277.

Ramsay BH. 1998. The interactive multisensor snow and ice mapping system. *Hydrol. Proc.* **12**: 1537–1546.

Rayner NA, Parker DE, Horton EB, Folland CK, Alexander LV, Rowell DP, Kent EC, Kaplan A. 2003. Global analyses of sea surface temperature, sea ice, and night marine air temperature since the late nineteenth century. *J. Geophys. Res.* **108**(D14): 4407 https://doi.org/10.1029/2002JD002670.

Robinson DA, Dewey KF, Heim RR. 1993. Global snow cover monitoring: an update. *Bull. Am. Meteorol. Soc.* **74**: 1689–1696.

Sceen JA, Simmonds I, Deser C, Tomas R. 2013. The atmospheric response to three decades of observed Arctic sea ice loss. *J. Clim.* **26**: 1230–1248.

Seager R, Kushnir Y, Nakamura J, Ting M, Naik N. 2010. Northern Hemisphere winter snow anomalies: ENSO, NAO and the winter of 2019/10. *Geophys. Res. Lett.* **37**: L14703. https://doi.org/10.1029/2010GL043830.

Shen X-S, Kimoto M. 2007. Studies of the interannual variability of spring Eurasian surface air temperature (in Chinese). *Chin. J. Atmos. Sci.* **31**: 19–27.

Smith TM, Reynolds RW. 2004. Improved extended reconstruction of SST (1854–1997). *J. Clim.* **17**: 2466–2477.

Sun CH, Song Y, Li WJ, Zhang RN, RG W. 2016. Interannual variations of the dominant modes of East Asian winter monsoon and possible links to Arctic sea ice. *Clim. Dyn.* **47**: 481–496.

Wadlland DJ, Simmonds I. 1997. Modeled atmospheric response to changes in Northern Hemisphere snow cover. *Clim. Dyn.* **13**: 25–34.

Wang HJ, Fan K. 2013. Recent changes in the East Asian monsoon. *Adv. Atmos. Sci*. **37**: 313–318.

Wang B, ZW W, Chang CP, Liu J, Li JP. 2010a. Another look at interannual-to-interdecadal variations of the East Asian winter monsoon: the northern and southern temperature modes. *J. Clim.* **23**: 1495–1512.

Wang HJ, Zhang Y, Lang XM. 2010b. On the prediction of short-term climate prediction. *Clim. Environ. Res.* **15**: 225–258.

Watanabe M, Nitta T. 1999. Decadal changes in the atmospheric circulation and associated surface climate variations in the Northern Hemisphere winter. *J. Clim.* **12**: 494–509.

Wu BY, Su JZ, Zhang RH. 2011. Effects of autumn-winter Arctic sea ice on winter Siberia high. *Chin. Sci. Bull.* **56**: 3220–3228.

Xiao D, Zhou XJ, Zhao P. 2012. Numerical simulation study of temperature change over East China in the past millennium. *Sci. China Earth Sci.* **55**: 1504–1517. https://doi.org/10.1007/s11430-012-4422-3.

Yang S, Lau K, Kim K. 2002. Variations of the East Asian jet stream and Asian-Pacific-American winter climate anomalies. *J. Clim*. **15**: 306–325.

Zhang R, Sumi A, Kimoto M. 1996. Impact of El Nino on the East Asian monsoon: a diagnostic study of the 86/87 and 91/92 events. *J. Meteorol. Soc. Jpn.* **74**: 49–62.

Zhao P, Jones P, Cao LJ, Yan ZW, Zha SY, Zhu YN, Yu Y, Tian GL. 2014. Trend of surface air temperature in eastern China and associated large-scale climate variability over the last 100 years. *J. Clim.* **27**: 4693–4703.

Zhu YF. 2008. An index of East Asian winter monsoon applied to description the Chinese mainland winter temperature changes (in Chinese). *Acta Meteoreol. Sin.* **66**: 781–788.

Zuo JQ, Ren H-L, Li WJ. 2015. Contrasting impacts of the Arctic oscillation on surface air temperature anomalies in southern China between early and middle-to-late winter. *J. Clim.* **28**: 4015–4026.

